Title

Targeting the MYC interaction network in B-cell lymphoma via histone deacetylase 6 inhibition

Running title

Targeting MYC in lymphoma via HDAC6 inhibition

Authors and affiliations

René Winkler[1*], Ann-Sophie Mägdefrau[1*], Markus Kleemann[1], Mandy Beyer[2], Kevin Linke[1], Lisa Hansen[1], Anna-Maria Schaffer[1,3], Marina E. Hoffmann[4], Simon Poepsel[5,6], Florian Heyd[7], Petra Beli[4], Tarik Möröy[8], Siavosh Mahboobi[9], Oliver H. Krämer[2], and Christian Kosan[1]

[1]Department of Biochemistry, Center for Molecular Biomedicine (CMB), Friedrich Schiller University Jena, Jena, 07745, Germany.

[2]Institute of Toxicology, University Medical Center Mainz, Mainz, 55131, Germany.

[3]Department of Immunology, Institute for Biology III, University of Freiburg, Freiburg, 79104, Germany.

[4]Institute of Molecular Biology (IMB), Mainz, 55128, Germany.

[5]Center for Molecular Medicine Cologne (CMMC), University of Cologne, Cologne, 50931, Germany.

[6]CECAD Research Center, Cologne, 50931, Germany.

[7]Institute of Chemistry and Biochemistry, Laboratory of RNA Biochemistry, Freie Universität Berlin, Berlin, 14195, Germany.

[8]Institut de Recherches Cliniques de Montréal (IRCM), Montréal, QC, H2W 1R7, Canada.

[9]Department of Pharmaceutical/Medicinal Chemistry I, Institute of Pharmacy, University of Regensburg, Regensburg, 93040, Germany.

*These authors contributed equally.

Keywords: MYC, HDAC6, B-cell lymphoma, HDAC inhibitor, heat-shock proteins

Additional information

Financial support

R.W. was supported by a scholarship from the Carl Zeiss Foundation. C.K. received funding from the Deutsche Forschungsgemeinschaft (DFG, German Research Foundation), GRK 1715. Work done in the group of O.H.K. was done by M.B. and funded by DFG, Project-ID 393547839 – SFB 1361 and DFG, GRK 2291/9-1.

Corresponding author

Christian Kosan, Department of Biochemistry, Center for Molecular Biomedicine (CMB), Friedrich Schiller University Jena, Hans-Knöll-Str. 2, Jena, 07745, Germany, christian.kosan@uni-jena.de, phone: +49 3641 949368.

Disclosure of conflicts of interest

The authors declare no potential conflicts of interest.

Text word count: **4662**

Abstract word count: **169**

Number of figures: **7**

Number of references: **50**

Abstract

Overexpression of oncogenic *MYC* is the hallmark of many lymphomas and is related to a poor prognosis. Although MYC is a potential cancer driver, therapeutic targeting is still challenging. Here, we report that histone deacetylase 6 (HDAC6) inhibition using the novel inhibitor Marbostat-100 (M-100) specifically alters protein-protein interactions in *MYC*-dependent cancer cells and targets MYC for proteasomal degradation. Subsequently, massive apoptosis is induced in *MYC*-overexpressing B-cell lymphoma cells after M-100 treatment. Besides, the application of M-100 prevents lymphoma formation in Eμ-Myc transgenic mice and efficiently slows down tumor growth in already manifested lymphomas. Moreover, M-100 exclusively targets *MYC*-dependent tumor cells with little or no side effects on non-tumor cells and tissues. HDAC6 inhibition results in pleiotropic cellular effects, such as hyperacetylation of Tubulin. We propose a mechanism where the heat-shock protein DNAJA3 associates with acetylated Tubulin to control MYC turnover in malignant cells. Our data show a new mechanism how HDAC6 inhibition targets oncogenic MYC in lymphomas and demonstrate a beneficial role of HDAC6 inhibition in *MYC*-dependent B-cell lymphoma.

Introduction

B-cells are prone to lymphomagenesis due to their high proliferative capacity and dependence on physiological DNA damage during V(D)J recombination and affinity maturation in germinal centers (1). Non-Hodgkin's lymphomas, such as Burkitt's lymphoma (BL) and diffuse large B-cell lymphoma (DLBCL) are aggressive heterogeneous lymphomas characterized by a difference in response to clinical treatment (2). BL is typically arising from germinal center B-cells and is often characterized by translocations of *MYC* to the vicinity of potent immunoglobulin enhancers, such as t(8;14) (1). DLBCL originates from various molecular alterations, among them translocations of BCL-6 or the anti-apoptotic factor BCL-2 (1). However, MYC translocations occur in around 15 % of DLBCL (2), and elevated expression of MYC is correlated with poor clinical outcome in B-cell lymphoma (3,4). Overexpression of the transcription factor MYC leads to fatal mis-regulations of cellular metabolism, cell growth, and signaling pathways (5,6). Moreover, MYC controls proliferation, angiogenesis, and mRNA processing in tumors (7,8). Oncogenic MYC can recruit epigenetic modifiers, such as p300/CBP or histone deacetylases (HDACs) HDAC1 and HDAC3 to activate or repress distinct genes in cancer cells (8).

Pan-HDAC inhibitors (HDACi) targeting several HDACs have been shown to give promising results in hematologic malignancies (9–11). The regulation of non-histone proteins, in particular proto-oncogenes, by HDACi enables the control of many essential cellular processes, such as cell survival, proliferation, protein stability, and protein interaction (12). For example, pan-HDACi treatment has been shown to inhibit BCL-6 function by inducing BCL-6 acetylation, which leads to the de-repression of its target genes (13). Interestingly, MYC can also be found acetylated at K423 upon pan-HDACi treatment, which decreases *MYC* transcription via autoregulation and results in apoptosis (10). Targeting singular HDACs with HDACi dissolves separate HDAC member function in hematologic malignancies. For example, treatment of DLBCL with the HDAC6 inhibitor ACY-1215 (Rocilinostat) activates the unfolded protein response by increasing quantity and acetylation of heat-shock proteins (HSPs), eventually resulting in cell death (14).

Importantly, oncogenic MYC has a half-life of about 35 min when transiently expressed (15). This high turn-over rate makes MYC a difficult target for direct inhibition. Attempts to

directly target MYC via small molecules did not achieve adequate results as these drugs underwent rapid degradation and showed unfavorably high IC_{50} values (16). In fact, physiological MYC fulfills crucial functions in many cell types, and pharmacological targeting of MYC should only counteract supraphysiological MYC levels in malignant cells to avoid severe side effects.

Here, we describe a novel targeting strategy for MYC-dependent B-cell lymphoma. The highly-specific HDAC6 inhibitor Marbostat-100 (M-100) induces degradation of oncogenic MYC and subsequent apoptosis in B-cell lymphoma, with little or no side effects on non-tumor cells and tissues. We uncover a cytoplasmic interaction network formed by Tubulin, HDAC6, and HSPs that regulates protein stability of oncogenic MYC. Our results extend current knowledge on MYC in B-cell lymphomagenesis and show a new approach to target oncogenic MYC in cancer.

Materials and methods

For detailed methods, please refer to the supplementary data.

In vivo animal studies

Female and male C57BL/6JRj and Tg(IghMyc)22Bri ("Eμ-Myc") mice with C57BL/6JRj background were housed in individually ventilated cages in groups under specific-pathogen-free conditions in the Experimental Biomedicine Unit at the University of Jena, Germany. Mice were bred according to registration number 02-053/16, and all experimental procedures were approved by the federal Thuringian "Landesamt für Verbraucherschutz" under registration number 02-030/15. All legal specifications were followed regarding European guidelines 2010/63/EU. Mice were randomly assigned to different treatment groups and sacrificed by cervical dislocation or CO_2 inhalation. For intraperitoneal injections, M-100 was solved in 7.5 % N-methyl-2-pyrrolidone (Carl Roth GmbH, Cat#P052) and 40 % PEG-400 (Carl-Roth, Cat#0144) in sterile water.

Cell lines and primary cultures

All cell lines were maintained in incubators at 37 °C and 5 % CO_2. 293T and NIH-3T3 cells were grown in DMEM with 10 % FCS. Ramos and Raji cells were grown in RPMI 1640 with 10 % FCS. BL-30 cells were grown in RPMI 1640 with 20 % FCS. OCI-Ly3, SUDHL-6, and CH12F3 cells were grown in RPMI 1640, supplemented with 10 % FCS, 50 μM β-mercaptoethanol, 10 mM HEPES. CH12F3 cells were activated by stimulation with 1 μg/ml CD40L (Thermo Fisher Scientific Inc., Cat#16-0402-81, RRID:AB_468944), 5 ng/ml IL-4 (Thermo Fisher Scientific Inc., Cat#14-8041-62) and 1 ng/ml TGF-β1 (Cell Signaling Technology, Cat#8915). All cell lines were tested regularly for *Mycoplasma* infection and only negatively tested cell lines were used. Isolation of primary B-cells was performed as previously described (17). Primary B-cells were grown in RPMI 1640 with 10 % FCS, 50 μM β-mercaptoethanol, 10 mM HEPES and 0.5 % gentamicin. Activation of primary B-cells was induced by the addition of 10 μg/ml LPS (from *E. coli*, O111:B4, Sigma-Aldrich Inc., Cat#L4391). Ramos cells were authenticated by Eurofins Genomics (Ebersberg, Germany). *MYC* mutation data are derived from the CCLE and COSMIC databases (18,19). M-100 was dissolved to a 10 mM stock solution with DMSO and diluted

to a concentration of 100 µM with PBS. Distribution of M-100 is restricted due to patent rights (patent number WO2016020369 A1).

Flow cytometry

All measurements were performed using a LSR Fortessa system (BD Biosciences Inc.), and data were acquired with BD FACSDIVA V8.0.1 (BD Biosciences Inc.). Immune cell phenotyping was performed by staining single-cell suspensions in PBS with respective antibodies (see Supplemental Data). For apoptosis detection, an Annexin V-FITC Apoptosis Detection Kit (Thermo Fisher Scientific Inc., RRID:AB_2575600) was used. Cell cycle analysis was performed by PI incorporation. Flow cytometry data were analyzed with FlowLogic 700.2A (Inivai Technologies Pty. Ltd.).

CRISPR/Cas9-mediated deletion of *HDAC6*

The CRISPR/Cas9-system was utilized to delete *HDAC6* in Ramos cells with the following crRNA: *GCCGGUUGAGGUCAUAGUUGGUUUUAGAGCUAUGCU*. Oligonucleotides Alt-R CRISPR-Cas9 tracrRNA, ATTO 550 (Integrated DNA Technologies, Inc., Cat#1075927) and Alt-R CRISPR-Cas9 crRNA (Integrated DNA Technologies, Inc.) were mixed for targeted deletion to a final duplex concentration of 100 µM, heated for 5 min at 95 °C and cooled down to RT. The formation of ribonucleoprotein complexes was achieved by mixing 120 pmol RNA duplex and 104 pmol Alt-R S. p. Cas9 Nuclease 3NLS (Integrated DNA Technologies, Inc., Cat# 1074181) with PBS to a final volume of 5 µl. The mixture was incubated for 20 min at RT and electroporated into Ramos cells using Cell Line Nucleofector Kit V (Lonza, Cat#VACA-1003) according to the manufacturer's protocol. In short, Ramos cells were washed once with PBS and resuspended in Nucleofector solution V. Then, ribonucleoprotein complexes and Alt-R Cas9 Electroporation Enhancer (Integrated DNA Technologies, Inc., Cat#1075915) were mixed with cells by pipetting, transferred to a cuvette and electroporation was performed in an Amaxa Nucleofector device (Lonza, program 0-06). Electroporated cells were resuspended in pre-warmed medium and cultivated. After 24 h, dead cells were eliminated using the Dead Cell Removal Kit (Miltenyi Biotec, Cat#130-090-101) according to the manufacturer's protocol. Electroporated cells were sorted after an additional 24 h using ATTO 550 label (BD FACSAria III, BD Biosciences Inc.), and expanded as single-cell

clones in 96-well plates. Proteins were separated with SDS-PAGE and analyzed using Western Blot to check for genomic deletion. The genomic region of interest was amplified by conventional PCR and sequenced (Eurofins Genomics).

RNA isolation

High-quality RNA was isolated using the Direct-zol RNA Miniprep Kit (Zymo Research, Cat#R2052). In short, cells were lysed in RNAPure peqGOLD (VWR International Ltd., Cat#30-1010) and mixed with an equal volume of 95 % (v/v) ethanol. RNA was bound to columns, washed, and subject to on-column-digestion with DNAse I (30 U; included in the kit) for 15 min at RT according to the manufacturer's protocol. RNA was eluted in RNAse-free water (included in the kit). The purity of RNA was measured by absorption at λ=230 nm, λ=260 nm, and λ=280 nm using a photometer (VWR International Ltd., ND-1000).

Quantitative real-time PCR

For quantitative real-time PCR experiments, cDNA was generated from up to 1 µg RNA using First Strand cDNA Synthesis Kit (Thermo Fisher Scientific Inc., Cat#K1612) according to the manufacturer's protocol, and an equally mixed combination of oligo-(dT)18 and random hexamer primers. Runs were performed on a StepOnePlus Real-Time PCR system (Thermo Fisher Scientific Inc.) using StepOne Software v2.3 (Life Technologies). PowerUp SYBR Green Master Mix (Thermo Fisher Scientific Inc., Cat#A25778) was combined with specific primers (200 pmol) and 5 ng cDNAs for a single reaction in 96-well plates (MicroAmp Fast Optical 96-well reaction plate, Applied Biosystems, Cat#4346906) sealed with MicroAmp Clear Adhesive Film (Applied Biosystems, Cat#4306311). Technical triplets and negative controls were prepared for each reaction. Polymerase started amplification after an initial denaturation step at 95 °C, and all annealing steps were performed at 60 °C. Melting curves were generated for each primer pair. Data analysis was performed using the comparative ΔΔCT method.

Proximity ligation assay

PLA was performed using Duolink In Situ PLA Reagents Red (Sigma Aldrich Inc., Cat#DUO92008) according to the manufacturer's protocol. Ramos cells were attached to coverslips with 0.1 % poly-L-lysine (Sigma Aldrich Inc., Cat#P8920) for 1 h at RT. Cells were permeabilized, fixed with methanol for 10 min at -20 °C, blocked with Duolink

blocking solution, and incubated with primary antibodies. PLA Probe Anti-Mouse MINUS (Sigma Aldrich Inc.) and PLA Probe Anti-Rabbit PLUS (Sigma Aldrich Inc.) were used as secondary probes. Samples were mounted with DAPI. PLA signals were detected using a Nikon Ti Microscope (λex=594 nm; λem=624 nm). Images were taken with a Nikon DS-Qi2 camera.

Cell fractionation

Cells were washed twice in PBS and centrifuged for 5 min at 700 g, RT. Then, pellets were resuspended in ice-cold cytoplasma extraction buffer (10 mM HEPES-KOH, pH 7.6, 15 mM KCl, 2 mM $MgCl_2$, 0.1 mM EDTA, freshly prepared 1 mM DTT, protease inhibitors) and incubated for 10 min on ice. Suspensions were centrifuged for 5 min at 700 g, RT, and supernatant (cytoplasmic extract) was collected. Residual pellets were washed twice in PBS and centrifuged for 5 min at 700 g, RT. Pellets were resuspended in ice-cold nuclear extraction buffer (20 mM HEPES-KOH, pH 7.9, 420 mM NaCl, 2 mM $MgCl_2$, 0.2 mM EDTA, 25 % (v/v) glycerin, 1 mM DTT; protease inhibitors) and incubated for 15 min at 4 °C. The supernatant (nuclear extract) was transferred into new reaction tubes after centrifugation for 10 min at 10000g and sonicated for 5 min using a water-bath sonicator (SONOREX SUPER RK106, Bandelin).

Immunoprecipitation

Protein levels were determined using the Roti-Nanoquant solution (Carl Roth GmbH, Cat#K880). For IPs, lysates containing 250 µg (overexpressed) or 1000 µg (endogenous) protein were combined with a mixture of 50 % (v/v) protein A and 50 % (v/v) protein G beads (Sigma-Aldrich Inc., Cat#P9424 and Cat#P3296) and 0.5-1 µg antibody in lysis buffer overnight at 4 °C. Following control antibodies were used: Mouse IgG control (Santa Cruz Biotechnology, Cat#sc-2025, RRID:AB_737182), Rabbit IgG control (Santa Cruz Biotechnology, Cat#sc-2027, RRID:AB_737197). Beads were washed three times in lysis buffer after incubation, resuspended in 2x Laemmli buffer to a final 1x concentration, and boiled for 5 min at 95 °C.

Results

HDAC6 inhibition increases the survival of lymphoma-prone Eμ-Myc mice.

Eμ-Myc mice are a commonly used model for studying the spontaneous formation of B-cell lymphomas due to B-cell-specific overexpression of *Myc*, resembling partially disease phenotypes of BL or DLBCL (20). To test the biological effect of the HDAC6 inhibitor M-100 on mice *in vivo*, we applied M-100 at 30 mg/kg or vehicle to 70-day-old wild-type or Eμ-Myc mice via intraperitoneal (i.p.) injection. Acetylation (Ac-) of the HDAC6 substrate Tubulin was increased in splenic cells 6 h and 72 h post treatment, indicating efficient HDAC6 inhibition (**Supplemental Figure 1A, B**). Short-term M-100 treatment did not change splenic B- and T-cell populations in Eμ-Myc and wild-type mice, and myeloid cells were only slightly reduced (**Supplemental Figure 1C-E**).

To study the long-term effect of M-100 on lymphomagenesis, 70-day-old Eμ-Myc mice that have a high incidence for lymphoma development (21), received i.p. injections with M-100 or vehicle twice a week for six weeks. Mice were monitored for another six weeks to check for spontaneous tumor formation after M-100 withdrawal. The survival of M-100-treated Eμ-Myc mice was significantly increased compared to vehicle-treated and untreated mice (**Figure 1A**). While 60 % of the vehicle-treated Eμ-Myc mice developed lymphomas during this period, only one out of 17 M-100-treated animals manifested a lymphoma. Interestingly, the beneficial effect of M-100 lasted even 6 weeks after M-100 withdrawal. Phenotyping of lymphomas from the vehicle group showed an expected 2:1 ratio of IgM^- to IgM^+ B-cell tumors (**Figure 1B**), as previously published (22). The mean spleen weight from the vehicle cohort was 265 mg compared to 120 mg from the M-100 cohort, indicating reduced disease progression (**Figure 1C**). Of note, long-term treatment with M-100 did not affect the body weight of mice (**Supplemental Figure 1F**). We analyzed lymphoid organs of surviving mice after the end of the experiment by flow cytometry. No differences were observed in B-cell populations between treatment groups because mice with increased percentage of B-cells showed lymphoma manifestation before reaching the defined endpoint (**Figure 1D**). However, survivors from the M-100 cohort showed a significant decline in myeloid cells and an increase in T-cells compared to the vehicle group (**Figure 1D**). Thus, shifted immune cell populations caused by long-term HDAC6 inhibition might prevent B-cell lymphomagenesis in Eμ-Myc mice.

Next, we assessed the curative potential of M-100 on already manifested lymphomas. We treated lymphoma-bearing Eμ-Myc mice with M-100 and analyzed their survival. Acute M-100 treatment significantly improved survival compared to receiving no treatment (**Figure 1E**). Taken together, long-term HDAC6 inhibition strongly reduces B-cell lymphomagenesis in mice overexpression *Myc*.

M-100 specifically induces apoptosis in lymphoma B-cells.

To test direct effects of M-100 on lymphoma cells, we treated purified B-cells from Eμ-Myc mice for 72 h with increasing amounts of M-100 (**Figure 2A**). Purified B-cells from wild-type mice were activated with 10 μg/ml LPS and served as control. B-cells from *Myc*-driven lymphomas showed a strong induction of apoptosis already after treatment with 1 μM M-100. Next, we determined the IC_{50} of M-100 on lymphoma B-cells from Eμ-Myc mice as 5.46 μM (**Figure 2B**). Interestingly, proliferating B-cells from wild-type mice did not undergo apoptosis after M-100 treatment (**Figure 2A**). We also assessed the effect of M-100 on the cell cycle of lymphoma cells and activated wild-type B-cells. Murine lymphoma cells showed a significant increase of cells in the subG1 fraction, indicating apoptosis, and a reduction in G1/S-phases 72 h after M-100 treatment (**Figure 2C**). However, non-malignant B-cells did not show any altered cell cycle progression (**Figure 2C**). Similarly, CH12F3 cells, a murine B-cell line harboring no *Myc* translocation (23), did not show increased subG1 fraction after M-100 treatment (**Figure 2D**).

On a molecular basis, we detected a strong acetylation of Tubulin concluding efficient Hdac6 inhibition by M-100 in murine B-cells from wild-type mice *ex vivo* (**Figure 2E**) which is a striking result as M-100 was developed against human HDAC6 (24,25). Wild-type B-cells upregulated the anti-apoptotic factor Bcl-2 in response to M-100 treatment (**Figure 2E**). However, Bcl-2 protein levels remained unchanged in Eμ-Myc lymphoma cells upon M-100 treatment (**Figure 2F**). Instead, Parp-1 cleavage, a marker of apoptosis, occurred 24 h after M-100 treatment in murine lymphoma cells (**Figure 2F**). Besides, transcription of *Bbc3* and *Pmaip1*, encoding pro-apoptotic Puma and Noxa, was increased and *Bcl-2* expression, measured for two transcripts, was decreased 24 h after M-100 treatment (**Figure 2G**). M-100 did not alter transcription of *Myc* (**Figure 2G**). Taken together, these findings clearly indicate that M-100 exclusively targets murine lymphoma cells with elevated Myc levels and induces apoptosis by preventing upregulation of Bcl-2.

HDAC6 inhibition induces apoptosis in human B-cell lymphoma cell lines.

We also wanted to assess the response of human B-cell lymphoma cell lines to M-100 in different BL and DLBCL cell lines. All used cell lines are characterized by *MYC* translocations or amplifications (26–31) but the individual *MYC* mutation profile differs heavily (**Figure 3A**). M-100 treatment resulted in a dose-dependent induction of apoptosis in human BL cell lines Ramos and Raji as demonstrated by the accumulation of Annexin V^+ cells (**Figure 3B**). In fact, all tested lymphoma cell lines showed a significant increase of Annexin V^+ cells after M-100 treatment (**Figure 3C**). We determined the efficacy of M-100 by MTT assay, and four out of five tested cell lines showed striking dose-responses to M-100 (**Figure 3D**). The obtained IC_{50} values ranged between 2.07 µM and 5.25 µM M-100. Raji cells, however, were less sensitive (IC_{50}=17.17 µM), although a substantial apoptosis induction was achieved at 4 µM M-100 (**Figure 3C**). Taken together, M-100 treatment resulted in cell death of a wide range of human *MYC*-dependent BL and DLBCL lymphoma cells.

Consistent with our findings from Eµ-Myc lymphoma cells, we detected a significant increase of subG1 fractions 72 h post M-100 treatment in human lymphoma cell lines (**Figure 3E**), and a reduced entry into S-phase already 24 h post treatment (**Supplemental Figure 2A, B**). Only BL-30 cells showed an unaltered cell cycle profile, which might be explained by the high mutation rate within the *MYC* gene (**Figure 3A, E**). To confirm the apoptotic response of lymphoma cells to M-100, combinatorial treatment of M-100 and the caspase-specific inhibitor Z-VAD-FMK was performed (**Supplemental Figure 2C**). The use of Z-VAD-FMK remarkably reduced the occurrence of early apoptotic cells in M-100-treated Ramos cells (**Supplemental Figure 2D**). This highlights again that cell death induction by M-100 is facilitated via the apoptotic pathway.

M-100 is a highly-specific HDAC6 inhibitor.

The HDAC6 inhibitor ACY-1215 is currently undergoing clinical trials but with modest results (32). We wanted to analyze if targeting properties of M-100 are superior to ACY-1215 and compared both inhibitors. ACY-1215 and M-100 caused a strong hyperacetylation of Tubulin in Ramos cells (**Figure 4A**). However, ACY-1215 treatment also resulted in off-target effects at 4 µM, such as histone H3 acetylation which was similar

to effects of the pan-HDACi MS-275 (**Figure 4A**). M-100 was highly specific at physiological concentrations and only a very weak histone H3 acetylation was detected at unphysiologically high concentrations (**Figure 4B**). Importantly, this limit is above most obtained IC_{50} values for M-100 in B-cell lymphoma cells (**Figure 2B, 3D**).

To further validate our findings, we generated Ramos HDAC6 knock-out (KO) cells using targeted CRISPR/Cas9 technology. HDAC6 KO cells were characterized by permanent hyperacetylation of Tubulin (**Figure 4C**). Importantly, KO of HDAC6 mimics to some extent the treatment with M-100 as Ramos HDAC6 KO cells showed reduced proliferation and increased apoptosis compared to cells containing HDAC6 (**Figure 4D, E**). As expected, Ramos HDAC6 KO cells were rather insensitive to M-100 treatment (IC_{50}=9.47 µM) as measured with MTT assay (**Figure 4F**). However, KO of HDAC6 barely altered the response of Ramos cells towards ACY-1215, revealing a very narrow window of specific targeting (**Figure 4F**). This underlines that M-100 has improved specificity for HDAC6 and preferentially induces acetylation of Tubulin but not off-targets such as histone H3.

HDAC6 inhibition induces MYC degradation.

MYC-dependent lymphoma cells respond to M-100 treatment with a strong induction of apoptosis. To shed further light on the underlying cellular mechanism, we treated Ramos cells with different concentrations of M-100 for 6 h and 24 h. MYC protein levels were already reduced 6 h after treatment with 2 µM and 4 µM M-100 (**Figure 5A**). Consistent with our previous findings, we also detected PARP-1 cleavage 24 h after treatment with M-100 (**Figure 5A**). Although BCL2 levels decreased after HDAC6 inhibition, we obtained opposing results for gene expression of the *BCL2* gene (**Figure 5B**). Expression of pro-apoptotic BIM was significantly upregulated, while *MYC* transcription again remained unaltered upon M-100 treatment (**Figure 5B**).

As we could observe apoptosis in *MYC*-dependent lymphoma cell lines upon M-100 treatment, we also tested Raji, BL-30, OCI-Ly3 and SUDHL-6 cells for their MYC levels after M-100 treatment. All tested BL and DLBCL cell lines showed a substantial reduction of MYC protein levels after 6 h (**Figure 5C**), pointing towards a general mechanism of MYC degradation after HDAC6 inhibition. To assess if MYC degradation is regulated by ubiquitin-mediated proteolysis upon HDAC6 inhibition, we performed combinatorial

treatments with M-100 and the proteasome inhibitor MG132. MYC degradation was efficiently blocked when proteasomes were not functioning (**Figure 5D**). These results indicate that HDAC6 inhibition by M-100 specifically provokes ubiquitination of MYC and subsequent proteasomal degradation.

MYC degradation is associated with changes in the interactome of Ac-Tubulin.

HDAC6 inhibition induces proteasomal degradation of MYC. To test whether this effect is mediated by a direct interaction, we performed immunoprecipitations (IPs) and were able to pull-down endogenous HDAC6/MYC complexes in Ramos cells (**Figure 6A**). However, HDAC6 is localized exclusively in the cytoplasm, whereas MYC is found in the cytoplasm and predominantly in the nucleus (**Figure 6B**). Thus, we analyzed the impact of MYC localization for its degradation. For this purpose, we transfected NIH-3T3 cells to express GFP-MYC and treated these cells with Importazole or Leptomycin B to block nuclear import or export, respectively (**Figure 6C**). Afterward, cells were treated with CHX to induce cell-intrinsic degradation and levels of MYC-GFP were tracked via flow cytometry. Interestingly, the degradation of MYC-GFP was significantly accelerated in the cytoplasm but not nucleus (**Figure 6C**).

It has been previously described that MYC is associated with Tubulin (33). As we showed that Tubulin is strongly acetylated in lymphoma cells after M-100 treatment, we wanted to detect the cytoplasmic localization of MYC in response to M-100. We detected a close localization between MYC and Ac-Tubulin in Ramos cells using proximity ligation assay (PLA), even under physiological conditions (**Figure 6D**). PLA signals disappeared after M-100 treatment, although MYC and Ac-Tubulin were still present (**Figure 6D**).

As Tubulin is an essential substrate of HDAC6, a detailed interactome analysis of heavily acetylated Tubulin was performed in *MYC*-dependent blood cancer cells via mass spectrometry. Bound proteins were identified which showed either increased abundance (>2-fold) or new binding to Ac-Tubulin after M-100 treatment compared to control. From 2309 identified proteins, treatment with M-100 led to enhanced binding of 357 proteins and new binding of 323 proteins to heavily acetylated Tubulin (**Figure 6E**). A functional annotation of the altered Tubulin interactome after M-100 treatment using the DAVID tool confirmed significant changes in proteins related to acetylation, nucleotide-binding,

protein transport, and ubiquitin conjugation (**Figure 6E**). Overrepresented protein groups that attached to heavily acetylated Tubulin were HSPs from the chaperone type, including DNAJ proteins (**Figure 6F**). For example, the chaperone member DNAJA3 which is important for proteasomal degradation and was shown to interact with MYC in high-throughput studies (34). Taken together, we demonstrated that MYC degradation is associated with changes in the interactome of Ac-Tubulin after HDAC6 inhibition.

The chaperone DNAJA3 is recruited to Ac-Tubulin and induces MYC degradation.

We verified the highly increased binding of DNAJA3 to Tubulin after M-100 treatment using overexpression studies (**Figure 7A**). In addition, we demonstrated the presence of Ac-Tubulin and DNAJA3 complexes endogenously in Ramos cells (**Figure 7B**). Of note, the chaperone DNAJA3 has large and small isoforms that are generated from the cleavage of precursor proteins (35,36), which we could also detect in our experiments (**Figure 7A, B**). We used PLA to uncover a close cellular localization of DNAJA3 with MYC in BL cells (**Figure 7C**). However, HDAC6 inhibition rapidly reduced the number of detected PLA foci per cell. These data suggest that heavily acetylated Tubulin acts as an interaction hub for MYC and DNAJA3 in the cytoplasm where degradation of MYC occurs.

As DNAJ proteins are involved in ATP-dependent protein folding and degradation (37), we investigated potential effects of DNAJA3 on MYC stability. Surprisingly, both DNAJA3 isoforms were able to significantly decrease high MYC levels in overexpression studies (**Figure 7D**). Finally, we retrospectively investigated the bone marrow of Eμ-Myc mice treated once by i.p. with 30 mg/kg M-100. Interestingly, we could detect elevated levels of DNAJA3 after M-100 treatment (**Figure 7E**) which could explain the observed absence of lymphomagenesis in *Myc*-driven mice. Taken together, our results indicate that HDAC6 inhibition (1) results in a remodeling of the Tubulin interactome driven by hyperacetylation, (2) recruitment of chaperones including DNAJA3 to Ac-Tubulin, and (3) degradation of oncogenic MYC in *MYC*-overexpressing cells (**Figure 7F**). Importantly, our results could be of beneficial use for the therapy of human *MYC*-dependent lymphoid malignancies.

Discussion

The role of HDAC6 inhibitors in cancer therapy is still a matter of debate. A recent study showed that many cancer models are tolerant to HDAC6 inhibitor treatment (38). However, a deeper look into the different tumor models in light of newly emerging inhibitors might be helpful in developing new strategies for cancer treatment. We demonstrate that *MYC*-dependent lymphomas are extremely sensitive to the highly-specific HDAC6 inhibitor M-100. HDAC6 was shown to preferentially target Tubulin dimers but also deacetylate microtubules at K40 (39). While Ac-Tubulin dimers showed reduced nucleation frequency, acetylated microtubules showed accelerated shrinkage (40). MYC is known to associate with microtubules that facilitate nuclear import of MYC by unknown mechanisms (33). Thus, microtubule acetylation might prevent transport of MYC to the nucleus and prolong cytoplasmic retention. In fact, we show that cytoplasmic localization of MYC promotes its proteasomal degradation.

The turn-over of MYC is depending on two opposing phosphorylation events of MYC at T58 and S62 which determines protein stability as a phosphodegron (41,42). Our data show that Raji cells which are mutated at T58 were the least sensitive to M-100. Thus, efficient MYC degradation after HDAC6 inhibition might require wild-type T58 in MYC. Interestingly, phosphorylation of MYC impeded its interaction with Tubulin, resulting in increased MYC stability in BL (41). Vice versa, our data indicate that the association of MYC with Ac-Tubulin decreases MYC stability. Moreover, our interactome data suggest that hyperacetylation of Tubulin leads to recruitment of proteins related to the functional annotation terms "Phosphoprotein", "Nucleotide-binding", and "Ubiquitin-like conjugation" which may influence the phosphodegron of MYC.

We did not discover effects of M-100 on direct acetylation sites of MYC in our experiments (data not shown). This observation is in contrast to the effects of the pan-HDACi MS-275 in hematological malignancies, where direct acetylation of MYC regulated target gene transcription (10). However, we were able to exclude direct transcriptional changes on *MYC* by M-100 in murine and human cells. This is underlined by several studies showing that M-100 treatment does not result in altered histone acetylation (43,25,44).

In our work we reveal that M-100 treatment of B-cell lymphoma cells induces proteasomal degradation of MYC. Besides, we prove that MYC forms a complex with the heat-shock protein DNAJA3 and hyperacetylation of Tubulin strongly recruits DNAJA3. Studies showed that DNAJA3 associates directly with the E3 ligase HUWE1 and von Hippel-Lindau tumor suppressor (45). HUWE1 is a major E3 ligase for MYC (46), which would connect DNAJA3 to the turnover of MYC. Besides, DNAJA3 was shown to mediate ubiquitination and degradation of oncogenic epidermal growth factor receptor (35). Previous strategies to inhibit HDAC6 using ACY-1215 in B-cell lymphoma resulted in an activation of the unfolded protein response by increasing quantity and acetylation of HSPs (14). Similarly, we observe increased levels of the HSP DNAJA3 in the bone marrow of mice treated with M-100. In addition, our interactome analysis suggest that HDAC6 inhibition leads to the recruitment of several DNAJ proteins to Ac-Tubulin, making it possible that other HSPs play a role in the observed MYC instability as well.

The occupation of MYC on distinct sets of target genes was described to depend on the amount of MYC molecules (5), which might explain the adverse Bcl-2 response of murine healthy and *Myc*-transformed B-cells to M-100 in our experiments. Eμ-Myc lymphoma cells treated with M-100 de-repressed *Bbc3* as well as *Pmaip1* and repressed *Bcl2* expression. Importantly, direct transcriptional regulation of *Bbc3* and *Pmaip1* by Myc was shown to be possible (47,48), and deficiency of *Bbc3* and *Pmaip1* accelerated lymphomagenesis in Eμ-Myc mice (49). Thus, permanent upregulation of *Bbc3* and *Pmaip1* caused by HDAC6 inhibition might be an explanation for the observed survival prolongation of Eμ-Myc mice upon long-term M-100 treatment.

Taken together, M-100 has potent anti-tumoral activity by targeting the stability of MYC. A fully water-soluble derivative of M-100 exists, which extends possible *in vivo* use (24). However, drug resistance to HDAC6 inhibition was recently described (50), and future directions should aim for rational drug combinations to treat distinct malignancies.

Acknowledgments

We thank Carmen Mertens for technical assistance as well as Dr. Karl-Gunther Glowalla, Petra Grübner and Andreas Köber for animal care. We are grateful to Katrin Schubert for assistance with cell sorting (FLI Jena) and Dr. David Corujo for bioinformatic support. We also want to thank Dr. Marcus Buschbeck for giving feedback on the manuscript. Prof. Dr. Ralf Küppers kindly provided lymphoma cell lines.

Authorship Contributions

Conception and design, C.K.; Development of methodology, R.W., A.-S.M., M.B., M.E.H., S.P., and F.H.; Acquisition of data, R.W., A.-S.M., M.K., M.B., K.L., L.H., A.-M.S., M.E.H., S.P., and F.H.; Analysis and interpretation of data, R.W., A.-S.M., M.E.H., and C. K.; Writing, review, and/or revision of the manuscript, R.W., A.-S.M., and C. K.; Administrative, technical, or material support, O.H.K., P.B., and S.M.; Study supervision, P.B., T.M, O.H.K., and C. K.

References

1. Basso K, Dalla-Favera R. Germinal centres and B cell lymphomagenesis. Nat Rev Immunol. Nature Publishing Group; 2015;15:172–84.

2. Swerdlow SH, Campo E, Pileri SA, Lee Harris N, Stein H, Siebert R, et al. The 2016 revision of the World Health Organization classification of lymphoid neoplasms. Blood. 2016;127:2375–90.

3. Gupta M, Maurer MJ, Wellik LE, Law ME, Han JJ, Ozsan N, et al. Expression of Myc, but not pSTAT3, is an adverse prognostic factor for diffuse large B-cell lymphoma treated with epratuzumab/R-CHOP. Blood. 2012;120:4400–6.

4. Aukema SM, Kreuz M, Kohler CW, Rosolowski M, Hasenclever D, Hummel M, et al. Biological characterization of adult MYC-translocation-positive mature B-cell lymphomas other than molecular Burkitt lymphoma. Haematologica. 2014;99:726–35.

5. Lorenzin F, Benary U, Baluapuri A, Walz S, Jung LA, von Eyss B, et al. Different promoter affinities account for specificity in MYC-dependent gene regulation. Elife. 2016;5:1–35.

6. Sabò A, Kress TR, Pelizzola M, De Pretis S, Gorski MM, Tesi A, et al. Selective transcriptional regulation by Myc in cellular growth control and lymphomagenesis. Nature. 2014;511:488–92.

7. Koh CM, Bezzi M, Low DHP, Ang WX, Teo SX, Gay FPH, et al. MYC regulates the core pre-mRNA splicing machinery as an essential step in lymphomagenesis. Nature. 2015;523:96–100.

8. Poole CJ, van Riggelen J. MYC—master regulator of the cancer epigenome and transcriptome. Genes (Basel). 2017.

9. Stubbs MC, Kim W, Bariteau M, Davis T, Vempati S, Minehart J, et al. Selective inhibition of HDAC1 and HDAC2 as a potential therapeutic option for B-ALL. Clin Cancer Res. 2015;21:2348–58.

10. Nebbioso A, Carafa V, Conte M, Tambaro FP, Ciro A, Martens J, et al. C-Myc modulation and acetylation is a key HDAC inhibitor target in cancer. Clin Cancer Res. 2016;23:2542–55.

11. Shin DY, Kim A, Kang HJ, Park S, Kim DW, Lee SS. Histone deacetylase inhibitor romidepsin induces efficient tumor cell lysis via selective down-regulation of LMP1 and c-myc expression in EBV-positive diffuse large B-cell lymphoma. Cancer Lett. Elsevier Ireland Ltd; 2015;364:89–97.

12. New M, Olzscha H, La Thangue NB. HDAC inhibitor-based therapies: Can we interpret the code? Mol Oncol. 2012;6:637–56.

13. Bereshchenko OR, Gu W, Dalla-Favera R. Acetylation inactivates the transcriptional repressor BCL6. Nat Genet. 2002;32:606–13.

14. Amengual JE, Johannet P, Lombardo M, Zullo K, Hoehn D, Bhagat G, et al. Dual

targeting of protein degradation pathways with the selective HDAC6 inhibitor ACY-1215 and bortezomib is synergistic in lymphoma. Clin Cancer Res. 2015;21:4663–75.

15. Salghetti SE, Kim SY, Tansey WP. Destruction of Myc by ubiquitin-mediated proteolysis: Cancer-associated and transforming mutations stabilize Myc. EMBO J. 1999;18:717–26.

16. Ross J, Miron CE, Plescia J, Laplante P, McBride K, Moitessier N, et al. Targeting MYC: From understanding its biology to drug discovery. Eur J Med Chem. 2021;213.

17. Winkler R, Kosan C. HDAC/HAT Function Assessment and Inhibitor Development. Methods Mol Biol. 2017;1510:93–101.

18. Barretina J, Caponigro G, Stransky N, Venkatesan K, Margolin AA, Kim S, et al. The Cancer Cell Line Encyclopedia enables predictive modelling of anticancer drug sensitivity. Nature. 2012;483:603–7.

19. Tate JG, Bamford S, Jubb HC, Sondka Z, Beare DM, Bindal N, et al. COSMIC: The Catalogue Of Somatic Mutations In Cancer. Nucleic Acids Res. Oxford University Press; 2019;47:D941–7.

20. Rempel RE, Jiang X, Fullerton P, Tan TZ, Ye J, Lau JA, et al. Utilization of the E -Myc Mouse to Model Heterogeneity of Therapeutic Response. Mol Cancer Ther. 2014;13:3219–29.

21. Ross J, Rashkovan M, Fraszczak J, Joly-Beauparlant C, Vadnais C, Winkler RR, et al. Deletion of the MIZ-1 POZ domain increases efficacy of cytarabine treatment in T- And B-ALL/lymphoma mouse models. Cancer Res. 2019;79:4184–95.

22. Schuster C, Berger A, Hoelzl MA, Putz EM, Frenzel A, Simma O, et al. The cooperating mutation or “second hit” determines the immunologic visibility toward MYC-induced murine lymphomas. Blood. 2011;118:4635–45.

23. Nakamura M, Kondo S, Sugai M, Nazarea M, Imamura S, Honjo T. High frequency class switching of an IgM+ B lymphoma clone CH12F3 to IgA+ cells. Int Immunol. 1996;8:193–201.

24. Leonhardt M, Sellmer A, Krämer OH, Dove S, Elz S, Kraus B, et al. Design and biological evaluation of tetrahydro-β-carboline derivatives as highly potent histone deacetylase 6 (HDAC6) inhibitors. Eur J Med Chem. 2018;152:329–57.

25. Sellmer A, Stangl H, Beyer M, Grünstein E, Leonhardt M, Pongratz H, et al. Marbostat-100 Defines a New Class of Potent and Selective Antiinflammatory and Antirheumatic Histone Deacetylase 6 Inhibitors. J Med Chem. 2018;61:3454–77.

26. Karpova MB, Schoumans J, Ernberg J, Henter JI, Nordenskjöld M, Fadeel B. Raji revisited: Cytogenetics of the original Burkitt’s lymphoma cell line. Leukemia. 2005;19:159–61.

27. Kleo K, Dimitrova L, Oker E, Tomaszewski N, Berg E, Taruttis F, et al. Identification of ADGRE5 as discriminating MYC target between Burkitt lymphoma

549 and diffuse large B-cell lymphoma. BMC Cancer. BMC Cancer; 2019;19:1–11.

550 28. Deng W, Clipson A, Liu H, Huang Y, Dobson R, Wang M, et al. Variable
551 Responses of MYC Translocation Positive Lymphoma Cell Lines To Different
552 Combinations of Novel Agents: Impact of BCL2 Family Protein Expression. Transl
553 Oncol. Elsevier Inc.; 2018;11:1147–54.

554 29. Bemark M, Neuberger MS. The c-MYC allele that is translocated into the IgH locus
555 undergoes constitutive hypermutation in a Burkitt's lymphoma line. Oncogene.
556 2000;19:3404–10.

557 30. Philip I, Philip T, Favrot M, Vuillaume M, Fontaniere B, Chamard D, et al.
558 Establishment of lymphomatous cell lines from bone marrow samples from
559 patients with burkitt's lymphoma. J Natl Cancer Inst. 1984;73:835–40.

560 31. Trabucco SE, Gerstein RM, Evens AM, Bradner JE, Shultz LD, Greiner DL, et al.
561 Inhibition of bromodomain proteins for the treatment of human diffuse large B-cell
562 lymphoma. Clin Cancer Res. 2015;21:113–22.

563 32. Amengual JE, Lue JK, Ma H, Lichtenstein R, Shah B, Cremers S, et al. First-in-
564 Class Selective HDAC6 Inhibitor (ACY-1215) Has a Highly Favorable Safety
565 Profile in Patients with Relapsed and Refractory Lymphoma. Oncologist.
566 2021;26:184-e366.

567 33. Alexandrova N, Niklinski J, Bliskovsky V, Otterson GA, Blake M, Kaye FJ, et al.
568 The N-terminal domain of c-Myc associates with alpha-tubulin and microtubules in
569 vivo and in vitro. Mol Cell Biol. 1995;15:5188–95.

570 34. Heidelberger JB, Voigt A, Borisova ME, Petrosino G, Ruf S, Wagner SA, et al.
571 Proteomic profiling of VCP substrates links VCP to K6-linked ubiquitylation and c-
572 Myc function. EMBO Rep. 2018;19:1–20.

573 35. Chen CY, Jan CI, Lo JF, Yang SC, Chang YL, Pan SH, et al. Tid1-L inhibits EGFR
574 signaling in lung adenocarcinoma by enhancing EGFR ubiquitinylation and
575 degradation. Cancer Res. 2013;73:4009–19.

576 36. Lu B, Garrido N, Spelbrink JN, Suzuki CK. Tid1 isoforms are mitochondrial DnaJ-
577 like chaperones with unique carboxyl termini that determine cytosolic fate. J Biol
578 Chem. 2006;281:13150–8.

579 37. Sterrenberg JN, Blatch GL, Edkins AL. Human DNAJ in cancer and stem cells.
580 Cancer Lett. Elsevier Ireland Ltd; 2011;312:129–42.

581 38. Depetter Y, Geurs S, De Vreese R, Goethals S, Vandoorn E, Laevens A, et al.
582 Selective pharmacological inhibitors of HDAC6 reveal biochemical activity but
583 functional tolerance in cancer models. Int J Cancer. 2019;145:735–47.

584 39. Miyake Y, Keusch JJ, Wang L, Saito M, Hess D, Wang X, et al. Structural insights
585 into HDAC6 tubulin deacetylation and its selective inhibition. Nat Chem Biol.
586 Nature Publishing Group; 2016;12:748–54.

587 40. Portran D, Schaedel L, Xu Z, Théry M, Nachury M V. Tubulin acetylation protects
588 long-lived microtubules against mechanical ageing. Nat Cell Biol. 2017;19:391–8.

589 41. Niklinski J, Claassen G, Meyers C, Gregory M a, Allegra CJ, Kaye FJ, et al.
590 Disruption of Myc-tubulin interaction by hyperphosphorylation of c-Myc during
591 mitosis or by constitutive hyperphosphorylation of mutant c-Myc in Burkitt's
592 lymphoma. Mol Cell Biol. 2000;20:5276–84.

593 42. Popov N, Schülein C, Jaenicke LA, Eilers M. Ubiquitylation of the amino terminus
594 of Myc by SCFβ-TrCPantagonizes SCFFbw7-mediated turnover. Nat Cell Biol.
595 2010;12:973–81.

596 43. Schäfer C, Göder A, Beyer M, Kiweler N, Mahendrarajah N, Rauch A, et al. Class
597 I histone deacetylases regulate p53/NF-κB crosstalk in cancer cells. Cell Signal.
598 Elsevier Inc.; 2017;29:218–25.

599 44. Stojanovic N, Hassan Z, Wirth M, Wenzel P, Beyer M, Schäfer C, et al. HDAC1
600 and HDAC2 integrate the expression of p53 mutants in pancreatic cancer.
601 Oncogene. Nature Publishing Group; 2017;36:1804–15.

602 45. Thompson JW, Nagel J, Hoving S, Gerrits B, Bauer A, Thomas JR, et al.
603 Quantitative Lys-ϵ-Gly-Gly (diGly) proteomics coupled with inducible RNAi reveals
604 ubiquitin-mediated proteolysis of DNA damage-inducible transcript 4 (DDIT4) by
605 the E3 Ligase HUWE1. J Biol Chem. 2014;289:28942–55.

606 46. Inoue S, Hao Z, Elia AJ, Cescon D, Zhou L, Silvester J, et al. Mule/Huwe1/Arf-BP1
607 suppresses Ras-driven tumorigenesis by preventing c-Myc/Miz1-mediated down-
608 regulation of p21 and p15. Genes Dev. 2013;27:1101–14.

609 47. Wirth M, Stojanovic N, Christian J, Paul MC, Stauber RH, Schmid RM, et al. MYC
610 and EGR1 synergize to trigger tumor cell death by controlling NOXA and BIM
611 transcription upon treatment with the proteasome inhibitor bortezomib. Nucleic
612 Acids Res. 2014;42:10433–47.

613 48. Maclean KH, Keller UB, Rodriguez-Galindo C, Nilsson JA, Cleveland JL. c-Myc
614 Augments Gamma Irradiation-Induced Apoptosis by Suppressing Bcl-XL. Mol Cell
615 Biol. 2003;23:7256–70.

616 49. Michalak EM, Jansen ES, Happo L, Cragg MS, Tai L, Smyth GK, et al. Puma and
617 to a lesser extent Noxa are suppressors of Myc-induced lymphomagenesis. Cell
618 Death Differ. Nature Publishing Group; 2009;16:684–96.

619 50. Amengual JE, Prabhu SA, Lombardo M, Zullo K, Johannet PM, Gonzalez Y, et al.
620 Mechanisms of acquired drug resistance to the HDAC6 selective inhibitor
621 ricolinostat reveals rational drug-drug combination with ibrutinib. Clin Cancer Res.
622 2017;23:3084–96.

623

Figures and figure legends

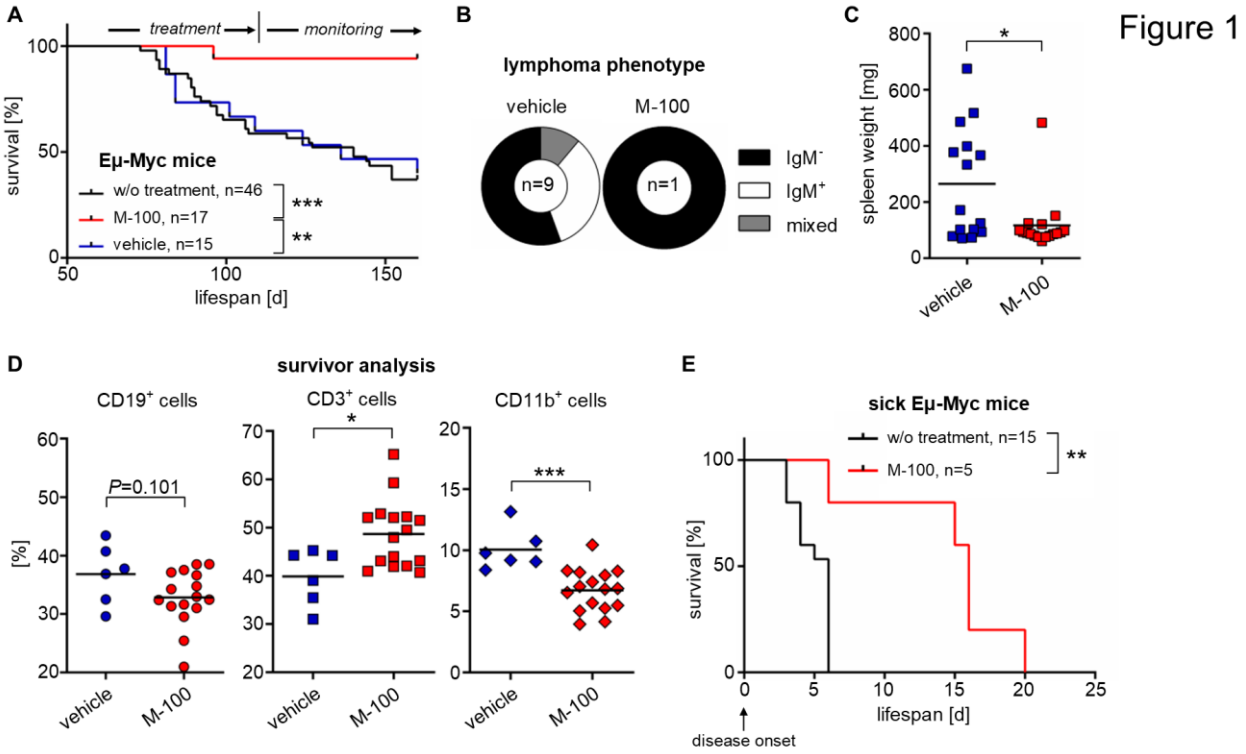

Figure 1: HDAC6 inhibition increases survival of lymphoma-prone Eμ-Myc mice.

(A) Survival curves of Eμ-Myc mice treated with 30 mg/kg M-100 or vehicle. Treatment started at age 70 d with two injections per week for six weeks. Afterward, mice were monitored for six weeks for signs of lymphoma development. The median survival of the vehicle cohort was 136 d, and the median survival of the M-100 cohort could not be determined for this experiment. In comparison, the survival curve of untreated Eμ-Myc mice (median 140 d) is shown. Log-Rank-test. **(B)** Lymphoma phenotypes were analyzed of diseased Eμ-Myc mice via flow cytometry using IgM surface expression. **(C)** Spleen weights were compared between all monitored mice reaching endpoint (death or end of the experiment). Each dot represents one mouse. Unpaired Student's t-test. **(D)** Flow cytometry analysis was performed of immune cell populations in spleens of survivors. Each dot represents one mouse. Unpaired Student's t-test. Bars depict mean. **(E)** Survival curves of Eμ-Myc mice suffering from an acute disease treated with M-100 (median 16 d) or left untreated (median 6 d). Mice were treated every 72 h with M-100 (30 mg/kg) starting when disease onset was present. Treatment continued until endpoint criteria were reached. Log-Rank-test. *P<0.05, **P <0.01, ***P<0.001.

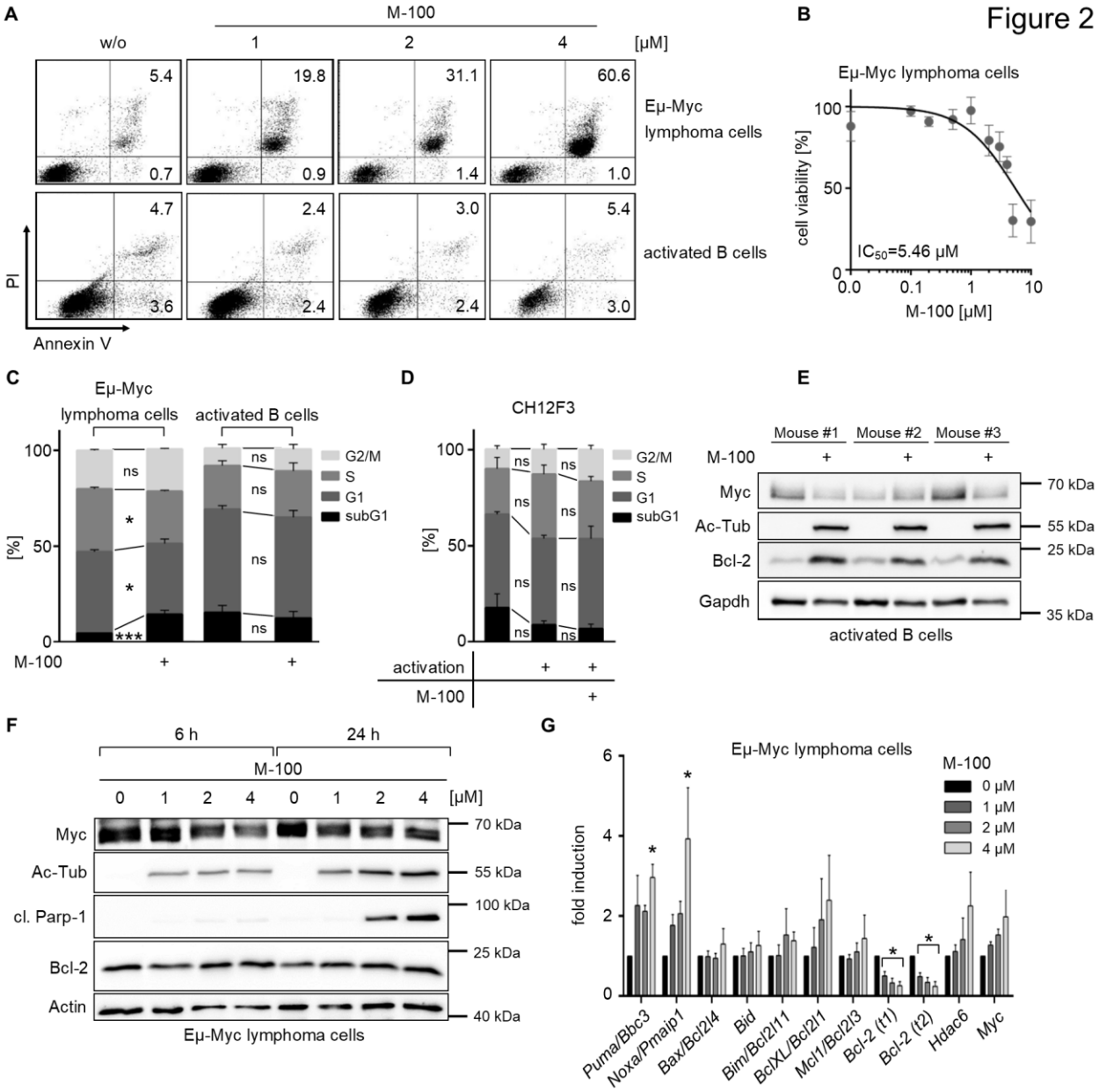

641 **Figure 2: M-100 specifically induces apoptosis in lymphoma B-cells.**

642 **(A)** Apoptosis was analyzed in Eµ-Myc lymphoma cells and activated (10 µg LPS/ml)
643 primary wild-type mouse B-cells treated for 72 h with 1 µM, 2 µM or 4 µM M-100 using
644 Annexin V and PI staining. **(B)** Cell viability was determined of Eµ-Myc lymphoma cells
645 treated for 48 h with increasing concentrations of M-100 using MTT assay. Non-linear
646 regression (inhibitor vs. normalized response) was inserted and IC_{50} was calculated. **(C)**
647 Cell cycle analysis of Eµ-Myc lymphoma cells and activated B-cells treated for 72 h with
648 4 µM M-100 was quantified. Two-Way ANOVA (Sidak's posthoc). **(D)** Cell cycle analysis

was performed of CH12F3 cells treated for 48 h with 2 µM M-100. Activation was performed using 1 µg/ml CD40L, 5 ng/ml IL-4, and 1 ng/ml TGF-β and added 2 h after M-100 treatment. CH12F3 cells harbor no *Myc* translocation. **(E)** Western Blot analysis was performed of activated wild-type B-cells from three individual mice stimulated with 10 µg/ml LPS for 18 h and 4 µM M-100 for additional 24 h. Gapdh was used as a loading control. Ac-Tub - acetylated Tubulin. **(F)** Western Blot analysis was performed of Eµ-Myc lymphoma cells treated for 6 h or 24 h with 1 µM, 2 µM or 4 µM M-100. Actin was used as a loading control. cl. - cleaved. **(G)** Gene expression was analyzed of Eµ-Myc lymphoma cells treated for 24 h with 1 µM, 2 µM or 4 µM M-100 using quantitative real-time PCR analysis. Fold inductions were calculated using the comparative ΔΔCT method based on *Actin* expression. Two different transcripts, t1 and t2, were analyzed for *Bcl2*. One-Way ANOVA (Dunnett's posthoc). Data in (A) - (D), (F), and (G) are representative of at least three independent experiments. All data represent mean + SEM, if applicable. **P*<0.05, ****P*<0.001, ns - not significant.

Figure 3

A

Cell line	*MYC* mutations	Type
Ramos°	translocated	BL
Raji	translocated p.YQ32del, p.S6T, p.E39D, p.A44V, **p.T58I**	BL
BL-30	translocated p.Q50H, p.T73I, p.G105D, p.S218N	BL
SUDHL-6	translocated	DLBCL
OCI-Ly3	amplified	DLBCL

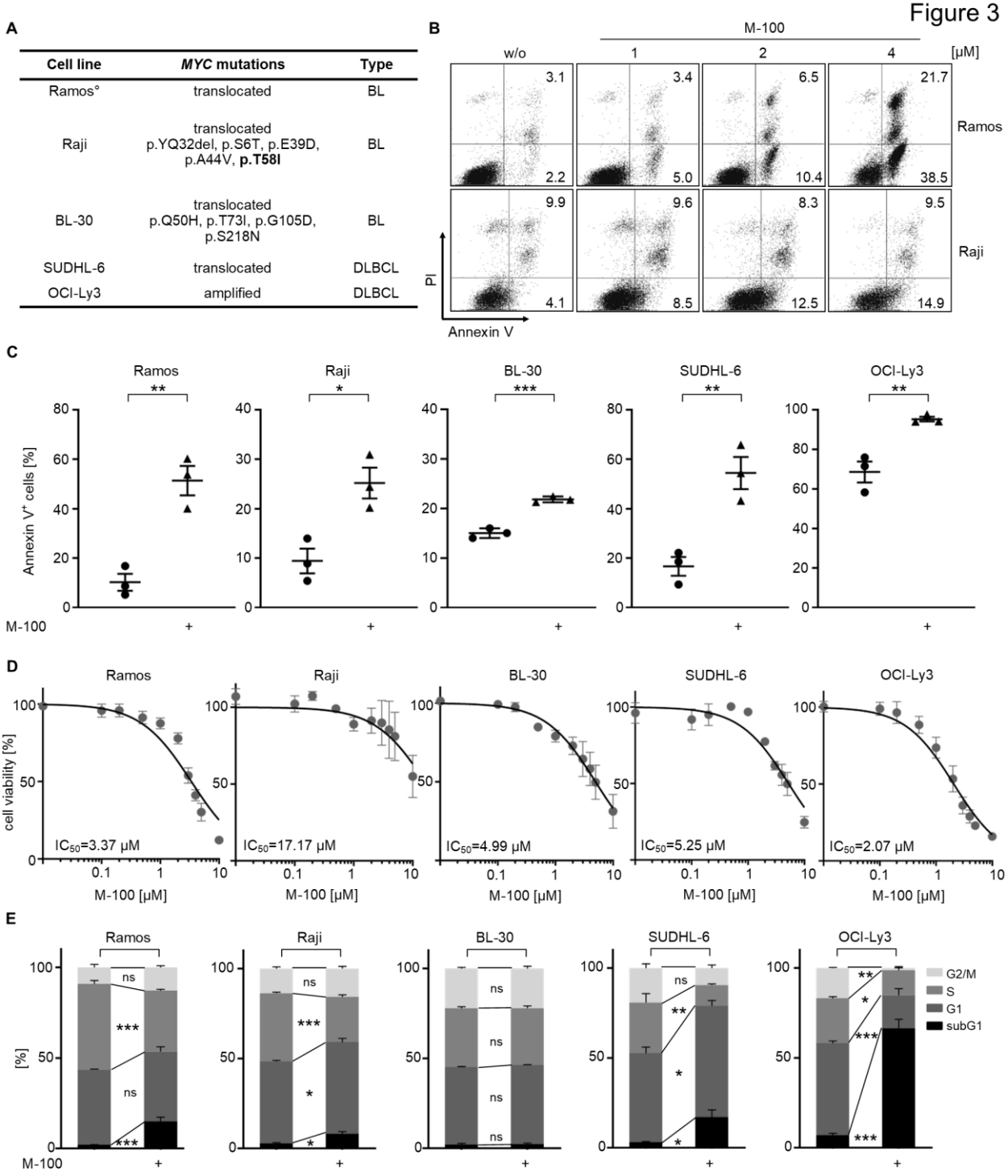

Figure 3: HDAC6 inhibition leads to apoptosis in human B-cell lymphoma cell lines.

(A) Table summarizing *MYC* mutations in the used cell lines from the CCLE and COSMIC databases. °Sequencing data were only available for subclone Ramos2G64C10. **(B)** Ramos and Raji cells were treated for 72 h with 1 µM, 2 µM or 4 µM M-100 and apoptosis

was analyzed by flow cytometry using Annexin V and PI staining. **(C)** The amount of Annexin V^+ cells was analyzed for the shown cell lines after treatment with 4 µM M-100 for 72 h. Unpaired Student's t-test. **(D)** Cells were treated for 48 h with increasing concentrations of M-100, and cell viability was determined using MTT assay. Non-linear regression (inhibitor vs. normalized response) was inserted and IC_{50} was calculated. **(E)** Cell cycle analysis was performed of cells treated as in (D). Two-Way ANOVA (Sidak's posthoc). Data in (B) - (E) are representative of at least three independent experiments. All data represent mean + SEM, if applicable. *P<0.05, **P <0.01, ***P<0.001, ns - not significant.

Figure 4

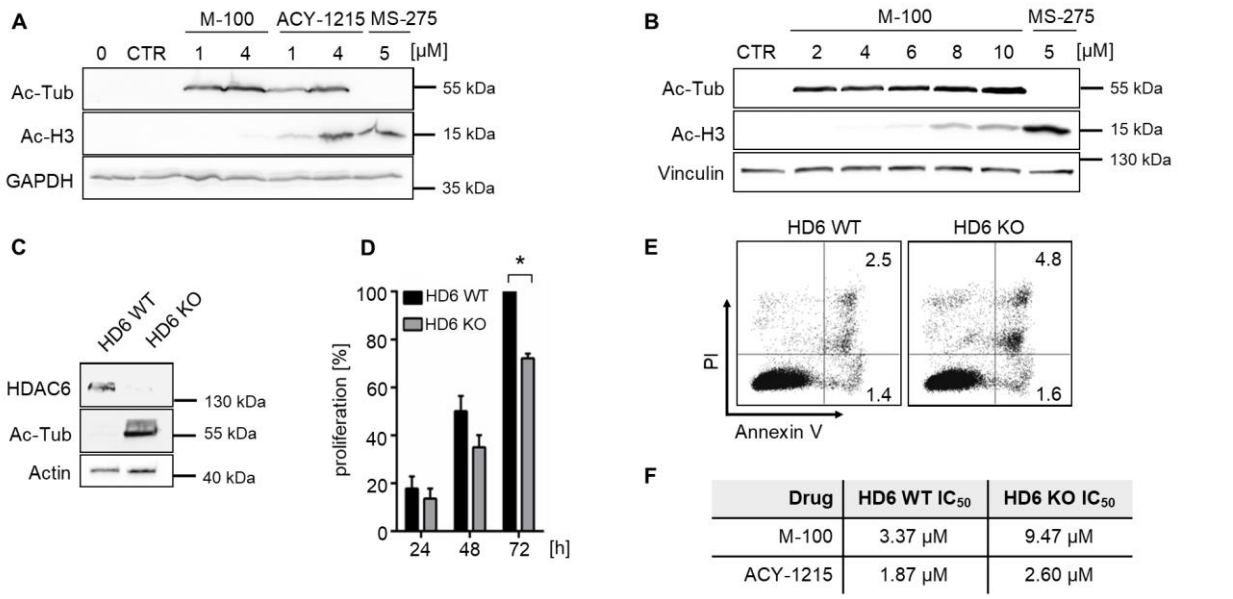

Figure 4: M-100 is a highly-specific HDAC6 inhibitor.

(A) Off-target effects were assessed for M-100 and ACY-1215 by comparing acetylated Tubulin (Ac-Tub) and acetylated histone 3 (Ac-H3) signals by Western blot. Treatment with pan-HDACi MS-275 serves as a control for Ac-H3 signals. All treatments were performed for 24 h. GAPDH was used as a loading control. **(B)** Different concentrations of M-100 were tested for inducing Ac-H3 signals by Western blot. Vinculin was used as a loading control. **(C)** Ramos HDAC6 (HD6) knock-out (KO) cells were generated and compared to HDAC6 wild-type (WT) cells. Western Blot analysis shows absence of HDAC6. Actin serves as a loading control. **(D)** Proliferation was measured of Ramos HDAC6 WT and Ramos HDAC6 KO cells by cell counting, and normalized to the value of Ramos HDAC6 WT cells at t=72 h. Two-Way ANOVA (Sidak's posthoc). **(E)** Apoptosis was analyzed in Ramos HDAC6 WT and Ramos HDAC6 KO cells using Annexin V and PI staining. **(F)** IC_{50} was determined for Ramos HDAC6 WT and Ramos HDAC6 KO cells treated for 48 h with M-100 or ACY-1215 by MTT assay. All data represent mean + SEM, if applicable. Data in (A) - (F) are representative of at least three independent experiments. *P<0.05.

Figure 5

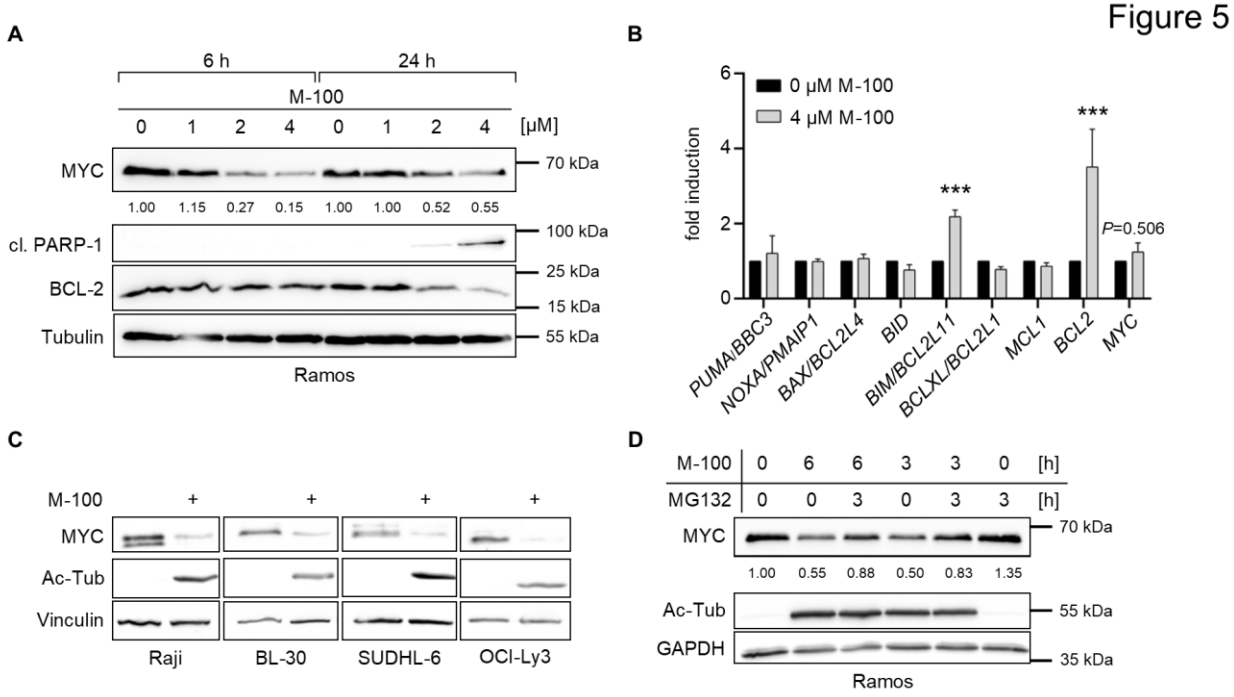

Figure 5: HDAC6 inhibition results in MYC degradation.

(A) Western Blot analysis was performed of Ramos cells treated for 6 h or 24 h with 1 µM, 2 µM or 4 µM M-100. Levels of MYC were quantified to untreated conditions. Tubulin was used as a loading control. cl. - cleaved **(B)** Gene transcription was analyzed of Ramos cells treated for 24 h with 4 µM M-100 using quantitative real-time PCR analysis. Fold inductions were calculated using the comparative ΔΔCT method based on *GAPDH* expression. Data represent mean + SEM. Multiple t-test. **(C)** Western Blot analysis was performed of indicated cell lines treated for 6 h or 24 h with 4 µM M-100. Vinculin was used as a loading control. Ac-Tub - acetylated Tubulin. **(D)** Western Blot analysis was performed of Ramos cells treated with 10 µM MG132 to block proteasomal degradation and/or 4 µM M-100 for the indicated time points. Levels of MYC were quantified to untreated conditions. GAPDH was used as a loading control. Data in (A) - (D) are representative of three independent experiments. ****P*<0.001.

Figure 6

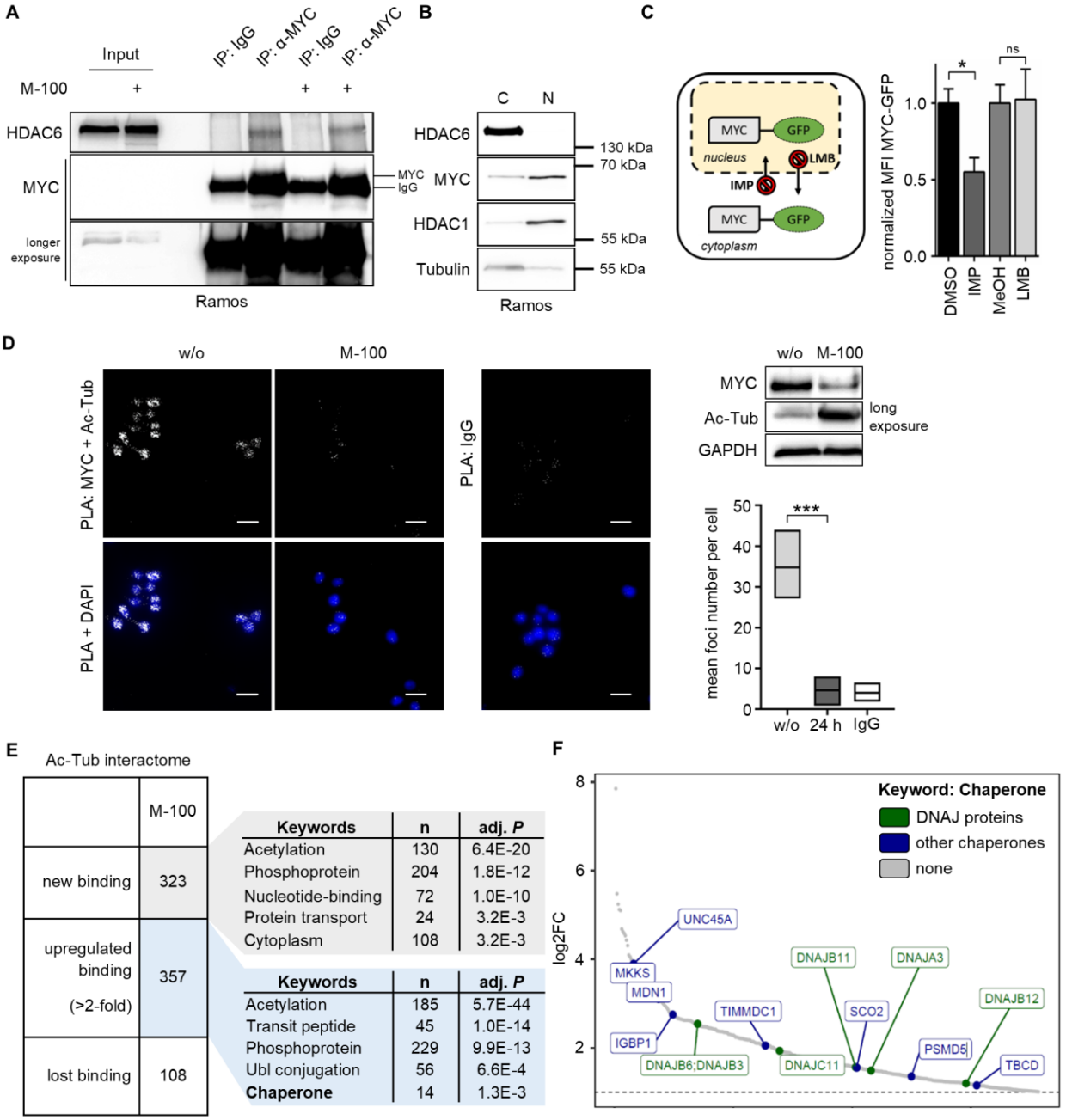

712 **Figure 6: Cytoplasmic MYC degradation is associated with changes in the**
713 **interactome of Ac-Tubulin.**

714 **(A)** Ramos cells were treated for 24 h with 4 µM M-100 or left untreated. Lysates were
715 used for IP with α-MYC antibodies and tested for HDAC6 interaction. IPs with unspecific
716 IgG were used as control. **(B)** Cytoplasmic and nuclear fractions were prepared from
717 Ramos cells. HDAC1 was used as a nuclear marker and Tubulin as a cytoplasmic marker.

(C) NIH-3T3 cells overexpressing MYC-GFP were challenged for 1 h with inhibitors of nuclear import (Importazole, IMP; 40 µM), nuclear export (Leptomycin B, LMB; 20 ng/ml) or solvent. Next, cells were treated for 90 min with CHX (50 µg/ml) before flow cytometry. Living cells were gated using FSC/SSC and normalized median fluorescence intensity (MFI) of MYC-GFP was calculated. Data represent mean + SEM. Unpaired Student's t-test. **(D)** PLA was performed to detect endogenous co-localization of MYC and Ac-Tubulin (Ac-Tub) in Ramos cells. Cells were treated with 4 µM M-100 for 24 h. Staining with unspecific IgG was used as a control. DAPI was used to stain nuclei. Scale bars indicate 20 µM. Western blot analysis depicts representative protein levels of MYC and Ac-Tub (long exposure) after 6 h M-100 treatment. PLA foci were counted and compared. One-Way ANOVA (Dunnett's posthoc). **(E)** Global interactome analysis was carried out of immunoprecipitated Ac-Tub via mass spectrometry. MV4-11 cells were treated for 24 h with 0.5 µM M-100. Shown are counts of proteins with new or increased (>2-fold) binding to Ac-Tub, or loss of binding after treatment compared to control and IgG binding. Uniprot (UP) keyword annotation was performed with DAVID using all proteins that bound to Ac-Tub after M-100 treatment. Adjusted (adj.) *P*-values are given. Ubl - Ubiquitin-like. **(F)** All proteins belonging to the keyword “Chaperone” are depicted with their corresponding log2 fold change (FC). DNAJ proteins are marked in green. Data in (A) and (C) are representative of three independent experiments. Data in (B) and (D) are representative of two independent experiments. **P*<0.05, ****P*<0.001.

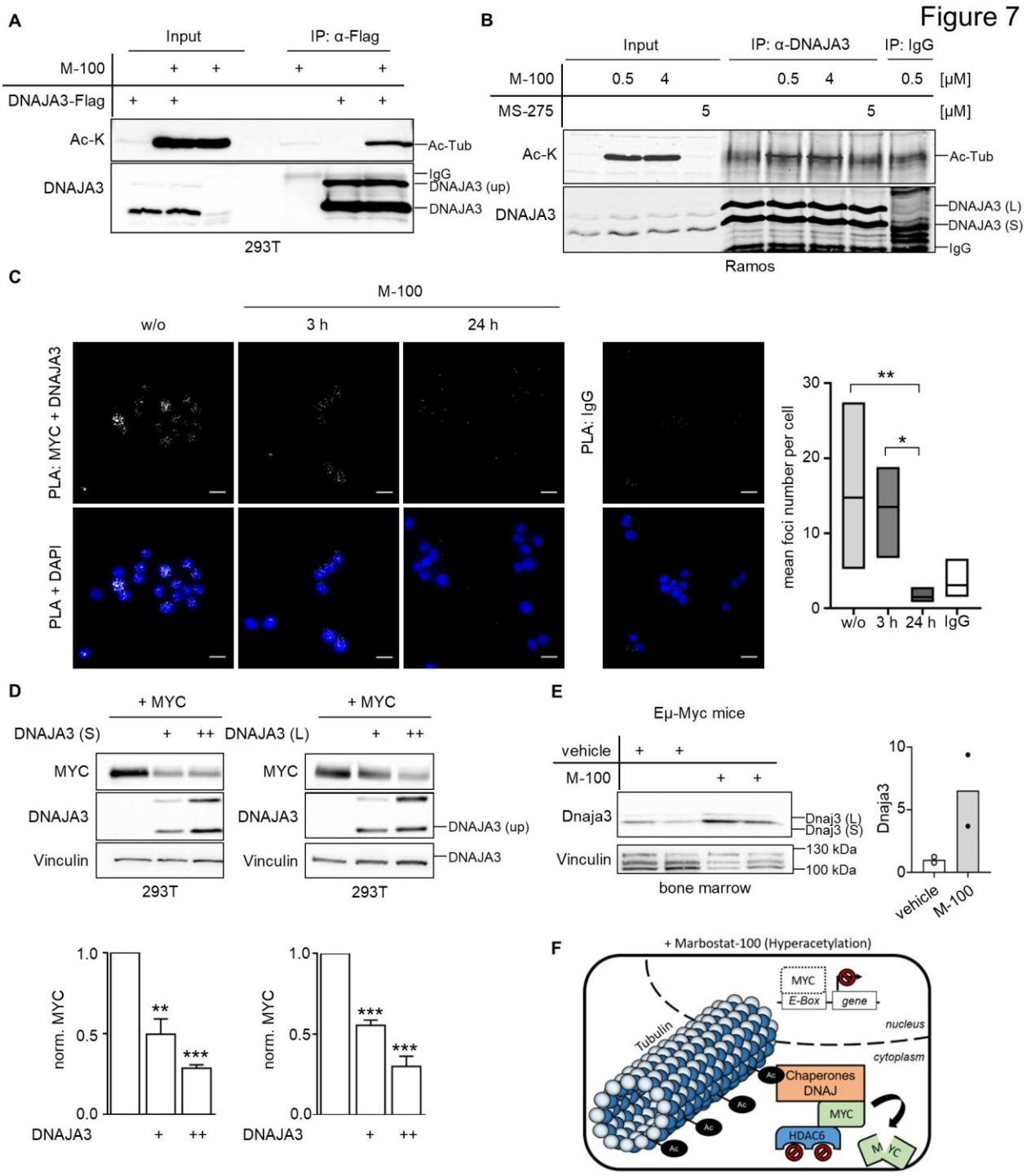

739 **Figure 7: The heat-shock protein DNAJA3 is recruited to hyperacetylated Tubulin**
740 **and induces MYC degradation.**

741 **(A)** 293T cells were transfected with plasmids encoding DNAJA3-Flag and were treated
742 for 24 h with 1 μM M-100 or left untreated. Cells were lysed in stringent lysis buffer

743 containing 1 µM M-100. Lysates were used for IP with α-Flag antibodies to precipitate
744 DNAJA3-Flag and tested for interaction with acetylated Tubulin (Ac-Tub). Overexpression
745 of DNAJA3 generates unprocessed (up) precursor proteins. **(B)** Ramos cells were treated
746 for 24 h with either 0.5 µM, 4 µM M-100, 5 µM MS-275, or left untreated. Lysates were
747 used for IP with α-DNAJA3 antibodies and tested for interaction with Ac-Tub. IPs with
748 unspecific IgG were used as control. **(C)** PLA was performed to detect endogenous co-
749 localization of MYC and DNAJA3 in Ramos cells. Cells were treated with 4 µM M-100 for
750 the indicated time points. Staining with unspecific IgG was used as a control. DAPI was
751 used to stain nuclei. Scale bars indicate 20 µM. PLA foci were counted and compared.
752 One-Way ANOVA (Dunnett's posthoc). **(D)** Western Blot analysis was performed of 293T
753 cells overexpressing increasing amounts of the small (S) or large (L) isoform of DNAJA3,
754 and MYC. Vinculin was used as a loading control. Quantification of MYC was performed
755 based on Vinculin. Data represent normalized mean + SEM. Unpaired Student's t-test. **(E)**
756 Western Blot analysis was performed of bone marrow lysates from Eµ-Myc mice after one
757 i.p. injection with M-100 (30 mg/kg) or vehicle. Small and large isoforms of Dnaja3 can be
758 noticed. Vinculin was used as a loading control. Each lane represents one individual
759 mouse. Quantification of Dnaja3 protein levels is shown based on Vinculin. **(F)** Scheme
760 summarizing our findings. Hyperacetylation of Tubulin by HDAC6 inhibition results in the
761 recruitment of Chaperone complexes including the heat-shock protein DNAJA3 to Tubulin.
762 High levels of DNAJA3 induce degradation of MYC. Data in (A), (B), and (D) are
763 representative of three independent experiments, data in (C) are representative of two
764 independent experiments. *P<0.05, **P<0.01, ***P<0.001.

765